Eur. Phys. J. Special Topics **167**, 3–10 (2009)
© EDP Sciences, Springer-Verlag 2009
DOI: 10.1140/epjst/e2009-00929-4

THE EUROPEAN PHYSICAL JOURNAL SPECIAL TOPICS

Regular Article

Structural properties of Ge/Si(001) nano-islands by diffraction anomalous fine structure and multiwavelength anomalous diffraction

M.-I. Richard[1,2], N.A. Katcho[3], M.G. Proietti[4], H. Renevier[5,a], V. Favre-Nicolin[1], Z. Zhong[6], G. Chen[6], M. Stoffel[7], O. Schmidt[7], G. Renaud[1], T.U. Schülli[1], and G. Bauer[6]

[1] INAC, CEA-Grenoble, France
[2] ID01/ESRF, Grenoble, France
[3] IQFR-CSIC, Dep. Quim. Inorganica – Universidad Complutense de Madrid, Spain
[4] ICMA, Dep. Fisica de la Materia Condensada, CSIC-Universidad de Zaragoza, Spain
[5] LMGP, Grenoble INP – Minatec, Grenoble, France
[6] Johannes Kepler Universität Linz, Institut für Halbleiter-und Festkörperphysik, Austria
[7] Institute for Integrative Nanosciences, IFW Dresden and MPI Stuttgart, Germany

Abstract. In the present paper, we aim to show the interest of combining Multiwavelength Anomalous Diffraction (MAD) and Diffraction Anomalous Fine Structure (DAFS) spectroscopy, in grazing incidence, to obtain structural properties (composition, strain and atomic ordering) of semiconductor heterostructures and nanostructures. As an example we report on preliminary results obtained on a series of Ge/Si(001) nano-island samples: pyramides and domes on nominal and prepatterned surfaces. For free standing domes, it is shown that the Ge content strongly depends on the growth condition with a tendency to increase from the bottom to the top of the nano-islands. There is also some indication of atomic ordering in the upper part of the islands. For small, capped pyramids, we show that the Diffraction Anomalous Fine Structure spectroscopy is the unique non destructive method that allows to recover the actual Ge content, the in-plane and out-of-plane strain and to detect atomic ordering.

1 Introduction

The knowledge of strain, chemical composition, interface quality, atomic ordering, *i.e.* structural properties at the long and short range scales, are of great importance to understand the growth mechanism as well as the electronic and optical properties of hetero and nanostructures [1]. To be suitable for devices, the nanostructures are encapsulated or embedded in a superlattice [2] and capping plays a decisive role by modifying the strain and possibly inducing atomic diffusion. Strain is closely related to composition, shape and aspect ratio of the nanostructures, and on the mutual stress which nanostructures, substrate and the matrix apply to each other.

X-ray diffraction is known to be a powerful tool for measuring strain fields and correlations [3]. On one side, X-ray Multiwavelength Anomalous Diffraction (MAD) allows to extract the scattering amplitude of the resonant and non resonant atoms. On the other side, X-ray Diffraction Anomalous Fine Structure (DAFS) spectroscopy allows to determine the local environment, as X-ray Absorption Fine Structure (XAFS) does, of resonant atoms located in an iso-strain volume selected by diffraction (spatial selectivity). The combination of both is a very powerful approach to disentangle strain and compostion. MAD records the diffracted intensity

[a] e-mail: hubert.renevier@inpg.fr

Table 1. Growth information of samples.

Sample	P_1	P_2	D_1	D_2
Substrate	patterned	patterned	flat	flat
Growth temperature (°C)	620	620	650	650
Ge deposition (MLs)	3.75	7	6	6
Average island diameter	88 nm	114 nm	110 nm	124 nm
Island type	{105} faceted pyramids	{111} faceted pyramids	domes	domes
Si capping layer	2 nm grown at 50 °C	–	–	–

in the reciprocal space at several energies close to the energy of an absorption edge. DAFS records the diffracted intensity, at fixed **Q** value in the reciprocal space, as a function of energy below and above an absorption edge, over an extended range of about 1000 eV with a step size of 1 to 4 eV. The Extended DAFS spectrum (EDAFS, oscillations above the edge) provides the chemical and electronic selectivity [4–6]. Both DAFS and MAD are non-destructive methods, which provide a statistical structural information, complementary to the very local imaging given by microscopy, and they can be applied also to the case of encapsulated nanostructures.

A major improvement of the DAFS spectroscopy is to perform the experiment in grazing incidence geometry (GIMAD and GIDAFS), to reduce the scattering contribution of the substrate, allowing to focus on the nanoobjects structural properties. In the past few years, grazing incidence MAD and DAFS has been applied to materials of great technological interest as semiconductors nanostructures, for instance InAs/InP(001) quantum wires [7,8], GaN/AlN(001) quantum dots [9–11], GeSi(001) [12]. A recent review can be found in Ref. [13], chapters 10 and 11.

In this report we focus on the results of our most recent work combining MAD and DAFS in grazing incidence to study Ge/Si(001) nano-islands. GeSi alloys have been widely studied, from the beginning of semiconductor research, on one side for device applications and integration on Si-based technology [14,15], and on the other, as a model system for semiconductor alloys. Since the nineties, research interest is being focused, as for other semiconductor systems, on laterally or vertically ordered 3D nanostructures [16]. Formation and evolution to different morphologies of GeSi QDs have been intensively investigated, strong changes are observed upon growth conditions, as fluxes [17], substrate temperature [18,19], Si capping [20]. This is a very suitable system to be studied by MAD/DAFS: a variety of different sizes and shapes with evolving faceting mechanisms (small {105} faceted pyramids, pyramids with dominant {111} facets, dome-shaped islands with {105}, {113} and {15 3 23} facets, barns [21], superdomes and flat-top superdomes [22]), a strong effect of Ge-Si intermixing giving different composition profiles [19,23,24], etc.

2 Results and discussion

2.1 Samples

We present here some preliminary results on Ge/Si(001) nano-islands. GIDAFS measurements have been performed for samples with different size and morphology or grown in different conditions. The Molecular Beam Epitaxy (MBE) growth of Ge on Si(001) was either on nominal or prepatterned surfaces. Prepatterning was obtained by lithography as described in Ref. [25]. The pit patterns of the prepatterned samples are two dimensionally ordered with a periodicity of ∼350–400 nm. The nucleation of islands on the prepatterned surfaces is described in detail in Ref. [26]. Four samples (P_1, P_2, D_1 and D_2) have been studied. The characteristics of their growth are summarized in Tab. 1. The grown islands exhibit either dome or pyramidal shape. The morphology of sample P_2 has been studied in detail in Ref. [27]. At the end of the growth of sample P_1, a 2 nm Si capping layer was deposited to prevent surface oxidation. We have

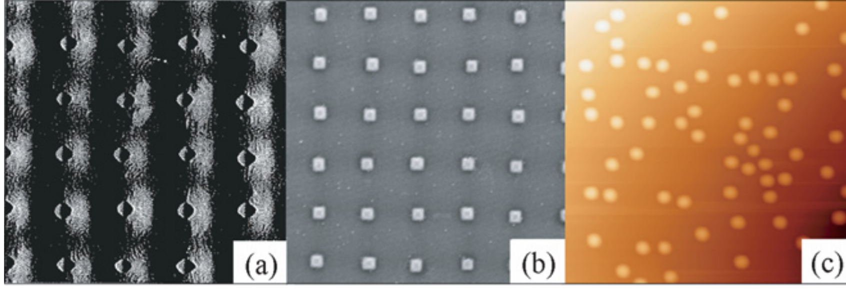

Fig. 1. $2 \times 2\,\mu\mathrm{m}^2$ AFM or SEM images of samples (a) P_1, (b) P_2, and (c) D_1.

experimentally observed with DAFS that a germanium oxide layer may rapidly form at the surface of GeSi islands in contact with atmospheric oxygen. A low temperature capping ($50\,^\circ$C) was used to preserve both the original morphology [28,29] and composition [30]. We show, in Fig. 1 the Atomic Force Microscopy (AFM) or Scanning Electron Microscopy (SEM) images of samples P_1, P_2 and D_1. The islands on sample P_1 are {105} faceted pyramids grown inside a 2D array of pits that are separated by saddle-like regions. The islands on sample P_2 are pyramids with dominant {111} facets in the upper part. The islands on samples D_1 and D_2 (not shown here) are regular domes.

2.2 Grazing incidence multiwavelength anomalous diffraction

MAD and DAFS measurements in Grazing Incidence were performed at beamline BM02 at the ESRF according to the experimental scheme described in previous papers [11,31]. A linear gas-detector (Vantec-1, Bruker) was used to record the scattered intensity. Grazing Incidence h-scans ($\alpha_c = 0.163\,^\circ$ at 11 keV), i.e. scan along surface in-plane direction $\langle$h00$\rangle$, were usually performed at 12 energies across the Ge K-edge (11103 eV), close to the in-plane Si(400) or Si(800) Bragg reflections. The scattered intensity was integrated over α_f in the range of 0 to about $1.5\,^\circ$. Then the modulus of Ge and Si structure factors ($|F_{Ge}|$, $|F_{Si}|$) and the phase difference $\varphi_{Si} - \varphi_{Ge}$ were recovered as a function of the reciprocal lattice unit h ($F_{Ge,Si}(hkl) = |F_{Ge,Si}(hkl)|\, e^{i\varphi_{Ge,Si}(hkl)}$). Figure 2 shows the results for the dome shaped sample D_2 grown on the Si(001) flat surface at $650\,^\circ$C.

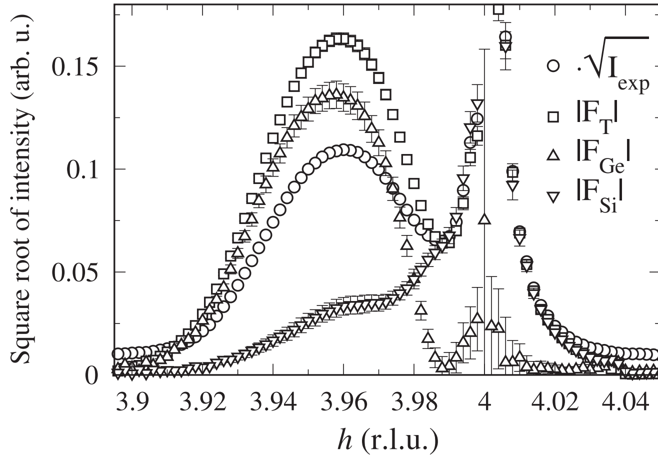

Fig. 2. $\sqrt{I_{exp}}$ measured at 11.053 keV (50 eV below Ge K-edge), $|F_T = F_{Ge} + F_{Si}|$, $|F_{Ge}|$ and $|F_{Si}|$ for dome shaped sample D_2 grown on nominal Si(001) surface ($\alpha_i = 0.15\,^\circ$, $\alpha_c = 0.163\,^\circ$ at 11 keV). F_{Ge} corresponds to the Thomson scattering of Ge atoms, F_{Si} corresponds to the Thomson and very weak anomalous scattering of Si atoms.

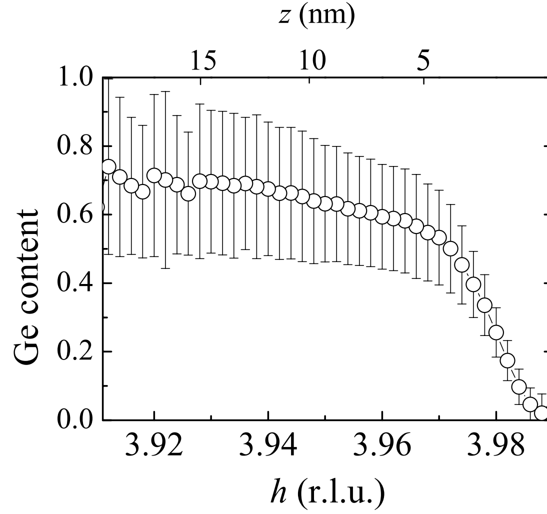

Fig. 3. Ge composition as a function of reciprocal unit h and z for dome shaped sample D_2 grown on nominal Si(001) surface, z is the height above the Si surface of the corresponding iso-strain region (see text).

The composition profile, as a function of h, is obtained in a straightforward way by using the following formula: $\frac{|F_{Ge}|}{|F_{Si}|} \approx \frac{x_{Ge} f^0_{Ge}}{(1-x_{Ge}) f^0_{Si}}$, where f^0_{Ge}(resp. f^0_{Si}) are the Ge (resp. Si) Thomson scattering and x_{Ge} the Ge concentration. It is shown in Fig. 3. In the frame of the Iso-Strain Scattering method [32], α_f (emergence angle) scans allow to relate h the height z above the Si surface of an iso-strain region of the quantum dots (QDs). In the following, Si reciprocal lattice unit (r.l.u.) are used. Figure 3 shows a steep increase of x_{Ge} for h in the range of 3.97 to 3.99, this effect is primarily attributed to the Si substrate contribution to the scattered intensity. Considering the Ge concentration for h lower than 3.97, the results clearly show a strong intermixing phenomenon leading to an island composition of about 60% Ge, together with a linear increase of Ge concentration from the bottom to the top of the dots. A DAFS spectrum was recorded at the Ge K-edge at a h value of 3.97 which corresponds to a z value of about (5 ± 1) nm. Figure 4 shows the DAFS spectrum measured together with a best fit obtained by refining $\beta_{SiGe} = \frac{|F_{Ge}|}{|F_{Si}|}$ and $\varphi_{Si} - \varphi_{Ge}$ in the following relation:

$$I_{exp} \propto D(E) \times \left[\left(\cos(\varphi_{Si} - \varphi_{Ge}) + \beta_{SiGe} \left(1 + \frac{f'_{Ge}}{f^0_{Ge}} \right) \right)^2 + \left(\sin(\varphi_{Si} - \varphi_{Ge}) + \beta_{SiGe} \frac{f''_{Ge}}{f^0_{Ge}} \right)^2 \right] \tag{1}$$

where *D(E)* is the detection efficiency. The EDAFS oscillations above the edge that show up in the fit curve originate from the experimental anomalous scattering factor f'_{Ge} and f''_{Ge} of bulk Ge and clearly do not fit the experimental oscillations. For $h = 3.97$ we obtain from β_{SiGe}, a Ge concentration $x_{Ge} 0.52 + -.01$, that is in good agreement with the MAD value, and a phase difference $\varphi_{Si} - \varphi_{Ge} = -0.66$ rad. In case of a homogeneous random alloy we should expect a phase difference close to zero since Si and Ge atoms fill in a random way equivalent cristallographic sites. If something like a phase segregation occurs one should deal instead with two different lattices, due to the inhomogeneous distribution of interatomic distances, *i.e.* lattice parameter, Ge and Si scattering contribution would be no longer scatter in phase. What could produce a non zero phase difference? The most straightforward explanations could be the following. First, the scattering contribution of strained Si substrate beneath the QD is not negligible for h value close to Si substrate reciprocal lattice unit ($h = 4$, for instance). Second, the presence of an out of plane Ge concentration gradient, as revealed by MAD. Atomistic simulations are in progress to quantify and distinguish these effects. Preliminary results have shown that both effects lead to non zero phase difference provided that the out of plane reciprocal unit l is away from zero by

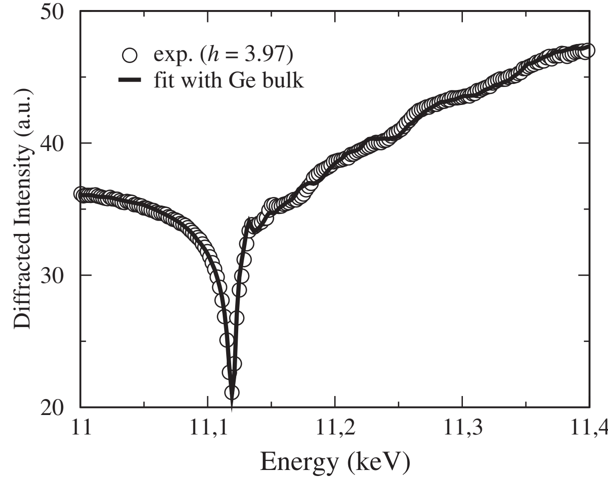

Fig. 4. Open circle: GIDAFS spectrum measured at $h = 3.97$ on the nominal part of sample D_2. Solid line: best fit performed with experimental f'_{Ge} and f''_{Ge} of a Ge thin film. The incident angle was set to $\alpha_i = 0.2°$, above the bulk Si critical angle $\alpha_c = 0.163°$ (at 11 keV).

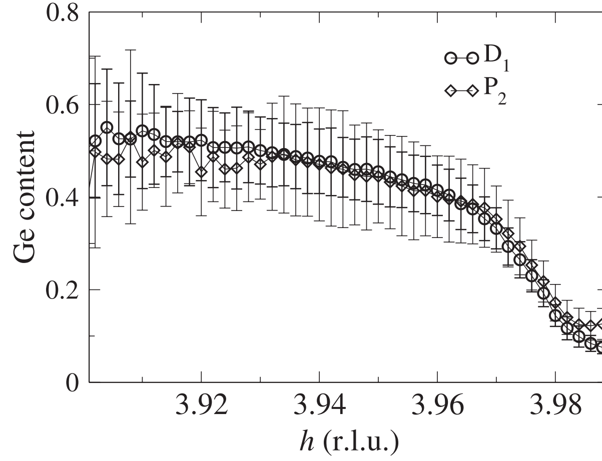

Fig. 5. Ge composition as a function of reciprocal unit h for dome, sample D_1 ($\alpha_i = 0.12°$) and pyramids with dominant {111} facets in the upper part, sample P_2 ($\alpha_i = 0.2°$).

only a few hundredths, that is Q_z is slightly non zero. The latter is always fulfilled in grazing incidence and exit geometry. Note that the phase difference is a model free parameter, that is related to the Ge and Si spatial distribution and therefore could help a lot to unveal this important aspect of the QD morphology.

In Figure 5, we show the Ge concentration profiles as a function of h, obtained by MAD for dome (D_1) and {111} faceted-pyramid (P_2) samples. For both cases the Ge concentration tends to stabilize at about 60%, as for dome sample D_2, with a similar h dependance.

2.3 Grazing incidence diffraction anomalous fine structure

Figure 6 shows the background-subtracted EDAFS spectrum of sample D_2 together with a number of theoretical EDAFS spectra obtained by atomistic simulations of relaxed cubic Ge-Si alloys with diamond structure. Calculations were performed using Monte Carlo (MC) simulations based on a Tersoff potential that is acknowledged to reproduce well the interatomic

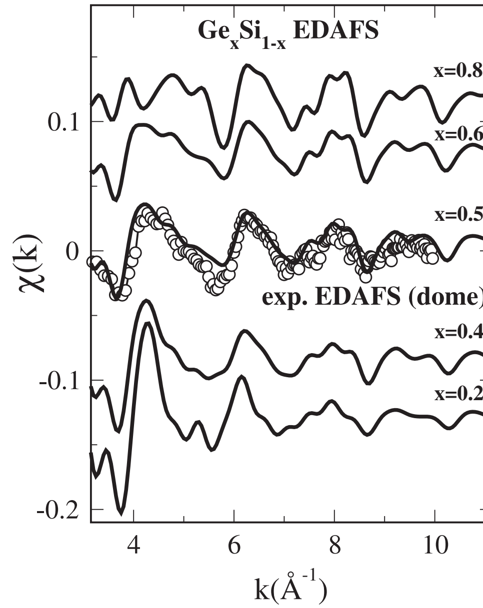

Fig. 6. Background-substracted EDAFS spectrum of sample D_2, corresponding to $h = 3.97$ ($z = (5 \pm 1)$ nm), together with theoretical EDAFS spectra obtained by atomistic simulations (MC) of relaxed Ge-Si alloys.

distances in semiconductors of group IV and III-V. Oscillations have been calculated starting from a 1000 atoms cluster, considering either a relaxed alloy supercell (Vegard's law) or pseudomorphic supercell, *i.e.* strained according to elasticity with the in-plane lattice parameter corresponding to the chosen h value ($a_{/\!/} = 0.547$ nm for $h = 3.97$). Theoretical phases and amplitudes were calculated using the Feff8.01 code [34], taking into account polarization and potential self-consistency for a sphere of 0.8 nm radius. Averaging of the different local environments was achieved by a random sampling of Ge atoms until convergence was reached (about 40 Ge absorbers). Simulations have been tested on Ge-Si relaxed alloys and pure Ge, providing correct interatomic distances and EXAFS shape. On figure 6 one can see the EDAFS oscillations showing remarkable changes with Ge/Si relative composition, which are more evident in the low k values range due to the very different backscattering function shape of Ge and Si. The purpose of figure 6 is to show the effect of composition and the qualitative agreement between EDAFS spectrum of sample D_2 and a 50% Ge-Si relaxed alloy. EDAFS oscillations for the pseudomorphic case of $Ge_{0.5}Si_{0.5}/Si(001)$ have also been calculated as an upper limit for strain, showing that the overall spectrum shape does not change, only subtle changes are observed. The quantitative EDAFS fit was performed with Ifeffit code [35] implemented by Artemis package [36]. The best fit results are shown in table 2, compared with bulk and relaxed alloy values of interatomic distances. The values found are close to the relaxed alloy, showing a partially relaxed Ge environment.

In figure 7 we shows the grazing incidence EDAFS oscillations corresponding to a series of samples. Quantitative analysis of the EDAFS spectra will be reported elsewhere in details. We can still mention here, qualitatively, that changes in the EDAFS shape from one case to the other are quite evident. Each spectrum, indeed, is qualitatively reproduced by different atomistic simulations. For sample D_1 we also have two EDAFS spectra recorded at $h = 3.93$ and $h = 3.965$ corresponding to different heights in the dot $z = (13 \pm 1)$ nm and $z = (9 \pm 1)$ nm, respectively. The different shapes are essentially reproduced by two main factors: Ge concentration and atomic ordering. The atomic ordering used in the simulations is the so-called RS2 model, that has been already observed by Malachias [33] associated to antiphase boundaries in GeSi domes. In sample D_1 we find a combination of an ordered phase and a 60% Ge random alloy for the upper part of the dot whereas the lower part of the dome looks more as a random 60% Ge

Table 2. EDAFS best fit results for domes (sample D_2), $h = 3.97$ ($z = (5 \pm 1)$ nm). Bond length values correspond to Ge nearest neighbor distances in nm, error bars are of the order of ± 0.001 nm (resp. ± 0.002 nm) for first nearest neighbor distance (resp. second nearest distance). *Monte Carlo simulation with Tersoff potential for a $Ge_{0.5}Si_{0.5}$ relaxed alloy with diamond structure.

bond length(nm)/Ge content(%)	Ge-Ge$_I$	Ge-Si$_I$	%Ge$_I$	Ge-Ge$_{II}$	Ge-Si$_{II}$	%Ge$_{II}$
bulk	0.245	0.235(Si-Si)	–	0.400	0.383(Si-Si)	–
dome	0.242	0.239	56	0.391	0.392	40
$Ge_{0.5}Si_{0.5}$ (relaxed alloy*)	0.2435	0.2402	50	0.3933	0.3921	50

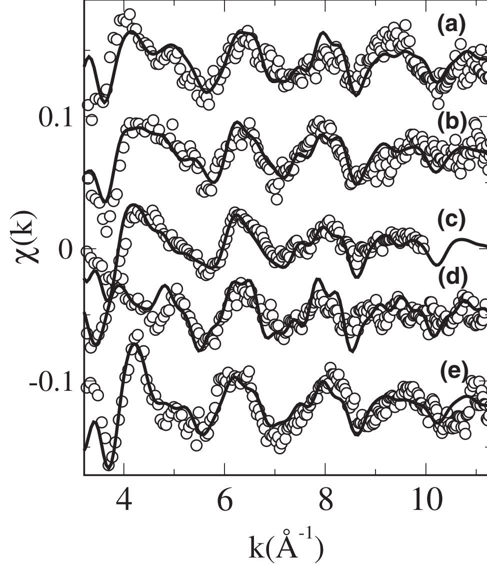

Fig. 7. Grazing incidence EDAFS oscillations corresponding to a series of samples together with Monte Carlo simulations (Tersoff potential). From top to bottom, (a, b) domes grown on Si nominal surface (sample D_1), (a) $h = 3.93$, $z = (13 \pm 1)$ nm and (b) $h = 3.965$, $z = (9 \pm 1)$ nm; (c) the sample previously shown $h = 3.97$, $z = (5 \pm 1)$ nm (D_2); (d) small pyramids with Si capping (P_1), $h = 7.97$ (e) pyramids with dominant {111} facets in the upper part (P_2), $h = 3.97$.

(as an average) alloy. Small capped pyramids are the closest to the RS2 ordered GeSi lattice corresponding to a 50% Ge concentration. The ordering phenomenon manifests as a Ge rich-like shape due to the higher number of Ge Nearest Neighbors (3 over 4 instead of 2). At last we show EDAFS of pyramidal domes showing a mixing of ordered and random phases.

3 Conclusion

In summary, we demonstrated that the combination of X-ray Multiwavelength Anomalous Diffraction (MAD) and X-ray Diffraction Anomalous Fine Structure (DAFS) spectroscopy is a very powerful approach to disentangle strain and compostion and to detect atomic ordering inside SiGe nanoislands. The further step to clarify and quantify the effects of growth conditions and morphology on the structural local properties of the QDs is performing atomistic simulation for a realistic model that can be compared to this complex mosaic of experimental results. Calculations are in progress.

We specially thank the ESRF for allocating beamtime and the BM02 staff for its help during the experiment.

References

1. J. Stangl, V. Holý, G. Bauer, Rev. Mod. Phys. **76**, 725 (2004)
2. Z. Yuan, B.E. Kardynal, R.M. Stevenson, et al., Science **295**, 102 (2002)
3. U. Pietsch, V. Holý, T. Baumbach, *High-resolution X-ray Scattering: From Thin Films to Lateral Nanostructures* (Springer Verlag, New York, 2004)
4. H. Stragier, J.O. Cross, J.J. Rehr, et al., Phys. Rev. Lett. **69**, 3064 (1992)
5. H. Renevier, J.-L. Hodeau, P. Wolfers, et al., Phys. Rev. Lett. **78**, 2775 (1997)
6. M.G. Proietti, H. Renevier, J.-L. Hodeau, et al., Phys. Rev. B **59**, 5479 (1999)
7. S. Grenier, M.G. Proietti, H. Renevier, et al., Europhys. Lett. **57**, 499 (2002)
8. A. Letoublon, V. Favre-Nicolin, H. Renevier, et al., Phys. Rev. Lett. **92**, 186101 (2004)
9. J. Coraux, V. Favre-Nicolin, M.G. Proietti, et al., Phys. Rev. B **73**, 205343 (2006)
10. J. Coraux, H. Renevier, V. Favre-Nicolin, et al., Appl. Phys. Lett. **88**, 153125 (2006)
11. J. Coraux, V. Favre-Nicolin, M.G. Proietti, et al., Phys. Rev. B **75**, 235312 (2007)
12. T.U. Schülli, J. Stangl, Z. Zhong, G. Bauer, et al., Phys. Rev. Lett. **90**, 066105 (2003)
13. C. Lamberti, *Characterization of Semiconductor Heterostructures and Nanostructures* (Elsevier Science, Amsterdam, 2008)
14. O.G. Schmidt, K. Eberl, IEEE Trans. Electr. Dev. **48**, 1175 (2001)
15. G.S. Kar, S. Kiravittaya, B.Y. Nguyen, et al., Appl. Phys. Lett. **88**, 253108 (2006)
16. D. Grützmacher, T. Fromherz, C. Dais, et al., Nano Lett. **7**, 3150 (2007)
17. M.-I. Richard, T.U. Schülli, G. Renaud, et al., Phys. Rev. B (2008) (submitted)
18. M. De Seta, G. Capellini, F. Evangelisti, Phys. Rev. B **77**, 045431 (2008)
19. T.U. Schülli, M. Stoffel, A. Hesse, et al., Phys. Rev. B **71**, 035326 (2005)
20. M. Stoffel, A. Rastelli, O.G. Schmidt, Surf. Sci. **601**, 3052 (2007)
21. M. Stoffel, A. Rastelli, J. Tersoff, et al., Phys. Rev. B **74**, 155326 (2006)
22. M.-I. Richard, G. Chen, T.U. Schülli, et al., Surf. Sci. **602**, 2157 (2008)
23. G. Katsaros, G. Costantini, M. Stoffel, et al., Phys. Rev. B **72**, 195320 (2005)
24. A. Rastelli, M. Stoffel, A. Malachias, et al., Nano Lett. **8**, 1404 (2008)
25. Z. Zhong, G. Bauer, Appl. Phys. Lett. **84**, 1922 (2004)
26. G. Chen, H. Lichtenberger, G. Bauer, et al., Phys. Rev. B **74**, 035302 (2006)
27. Z. Zhong, W. Schwinger, F. Schäffler, et al., Phys. Rev. Lett. **98**, 176102 (2007)
28. A. Rastelli, E. Müller, H. von Känel, Appl. Phys. Lett. **80**, 1438 (2002)
29. M. Stoffel, U. Denker, G.S. Kar, et al., Appl. Phys. Lett. **83**, 2910 (2003)
30. J. Stangl, A. Hesse, V. Höly, O.G. Schmidt, et al., Appl. Phys. Lett. **82**, 2251 (2002)
31. H. Renevier, S. Grenier, S. Arnaud, et al., J. Synchrotron Radiat. **10**, 435 (2003)
32. I. Kegel, T.H. Metzger, A. Lorke, et al., Phys. Rev. B **63**, 035318 (2001)
33. A. Malachias, T.U. Schülli, G. Medeiros-Ribeiro, et al., Phys. Rev. B **72**, 165315 (2005)
34. A.L. Ankudinov, et al., Phys. Rev. B **58**, 7565 (1998)
35. M. Newville, et al., Physica B **208-209**, 154 (1995)
36. B. Ravel, M. Newville, J. Synchrotron Radiat. **12**, 537 (2005)